Phys. Med. Biol. **57** (2012) 5823–5840 doi:10.1088/0031-9155/57/18/5823

In-bore setup and software for 3T MRI-guided transperineal prostate biopsy

Junichi Tokuda[1], Kemal Tuncali[1], Iulian Iordachita[2], Sang-Eun Song[1], Andriy Fedorov[1], Sota Oguro[1], Andras Lasso[3], Fiona M Fennessy[1], Clare M Tempany[1] and Nobuhiko Hata[1]

[1] Department of Radiology, Brigham and Womens Hospital and Harvard Medical School, Boston, MA, USA
[2] Laboratory for Computational Sensing and Robotics, Johns Hopkins University, Baltimore, MD, USA
[3] School of Computing, Queen's University, Kingston, ON, Canada

E-mail: tokuda@bwh.harvard.edu

Received 24 February 2012, in final form 18 July 2012
Published 5 September 2012
Online at stacks.iop.org/PMB/57/5823

Abstract

MRI-guided prostate biopsy in conventional closed-bore scanners requires transferring the patient outside the bore during needle insertion due to the constrained in-bore space, causing a safety hazard and limiting image feedback. To address this issue, we present our custom-made in-bore setup and software to support MRI-guided transperineal prostate biopsy in a wide-bore 3 T MRI scanner. The setup consists of a specially designed tabletop and a needle-guiding template with a Z-frame that gives a physician access to the perineum of the patient at the imaging position and allows the physician to perform MRI-guided transperineal biopsy without moving the patient out of the scanner. The software and Z-frame allow registration of the template, target planning and biopsy guidance. Initially, we performed phantom experiments to assess the accuracy of template registration and needle placement in a controlled environment. Subsequently, we embarked on our clinical trial ($N = 10$). The phantom experiments showed that the translational errors of the template registration along the right–left (RP) and anterior–posterior (AP) axes were 1.1 ± 0.8 and 1.4 ± 1.1 mm, respectively, while the rotational errors around the RL, AP and superior–inferior axes were $(0.8 \pm 1.0)^\circ$, $(1.7 \pm 1.6)^\circ$ and $(0.0 \pm 0.0)^\circ$, respectively. The 2D root-mean-square (RMS) needle-placement error was 3 mm. The clinical biopsy procedures were safely carried out in all ten clinical cases with a needle-placement error of 5.4 mm (2D RMS). In conclusion, transperineal prostate biopsy in a wide-bore 3T scanner is feasible using our custom-made tabletop setup and software, which supports manual needle placement without moving the patient out of the magnet.

(Some figures may appear in colour only in the online journal)

1. Introduction

MR-guided prostate biopsy is becoming an established approach to sample the gland (Cormack *et al* 2000, D'Amico *et al* 2000, Hata *et al* 2001, Susil *et al* 2004, Menard *et al* 2004, Krieger *et al* 2005, Zangos *et al* 2005, Susil *et al* 2006, Engelhard *et al* 2006, Blumenfeld *et al* 2007, de Oliveira *et al* 2008, Hambrock *et al* 2008, Rea *et al* 2008, Menard *et al* 2010, 2011, Yakar *et al* 2011, Zangos *et al* 2011, Schouten *et al* 2012). While transrectal ultrasound (TRUS) (Hodge *et al* 1989, Scherr *et al* 2002) is the most commonly used imaging modality to guide core needle prostate biopsy in the United States, the limited negative predictive value of the TRUS-guided systematic biopsy has been argued; several studies have demonstrated that the classic sextant biopsy found only 77–80% of cancers (Roehl *et al* 2002, Presti *et al* 2003, 2000). These false-negative biopsy specimens and rising PSA levels lead to repeated biopsies, frustrating both patients and clinicians. Compared to US, MRI provides excellent visualization of the prostate gland with its substructures, focal lesions within the gland and surrounding periprostatic tissues and is widely believed to be the ideal modality for imaging prostate cancer (Beyersdorff *et al* 2002). In the recent years, researchers have been investigating the clinical utility of MRI for targeted biopsy by fusing the preprocedurally acquired MRI with the intra-procedural US (Ukimura *et al* 2010, Natarajan *et al* 2011) or by means of intraoperative MRI for needle and anatomy visualization (Cormack *et al* 2000, D'Amico *et al* 2000, Hata *et al* 2001, Beyersdorff *et al* 2002, Susil *et al* 2003, 2004, Menard *et al* 2004, Krieger *et al* 2005, Zangos *et al* 2005, Susil *et al* 2006, Engelhard *et al* 2006, Blumenfeld *et al* 2007, de Oliveira *et al* 2008, Hambrock *et al* 2008, Rea *et al* 2008, Lakosi *et al* 2009, Oguro *et al* 2009, Menard *et al* 2010, 2011, Yakar *et al* 2011, Zangos *et al* 2011, Schouten *et al* 2012). While US-guided biopsy has been emerging because of its availability, portability, and the recent progress in imaging quality of US, MRI-guided biopsy has the advantages of better soft tissue contrast and applicability to patients who cannot undergo TRUS-guided biopsy due to previous total colectomy.

The type of needle-placement approach, either transrectal or transperineal, is an important factor that affects applicability to patients, accessibility to targets in the prostate gland and invasiveness in MRI-guided prostate biopsy. While devices to support transrectal approach has commercially been available and have been used in several clinical studies (Beyersdorff *et al* 2002, Engelhard *et al* 2006), the transperineal approach has also been investigated because of its better access to anterior and apical regions (Sartor *et al* 2008) and its applicability to patients, who cannot undergo TRUS-guided biopsy due to previous total colectomy. MRI-guided transperineal biopsy was first reported by D'Amico *et al* using an open-configuration 0.5 T MRI scanner (D'Amico *et al* 2000, Cormack *et al* 2000, Hata *et al* 2001). The open-configuration MRI magnet was ideal for transperineal approach, since it allowed the radiologist direct access to the patient's perineum in lithotomy position in the magnet throughout the procedure. As the subject stayed in the scanner, real-time MRI allowed monitoring the needle continuously during the needle-insertion process, significantly improving the accuracy of the needle placement and hence targeting.

The successful demonstration of MRI-guided transperineal prostate biopsy in this unique 0.5 T MRI scanner led other groups to investigate the use of conventional closed-bore scanners also for transperineal biopsy to take advantage of better image quality and wider availability of those scanners (Susil *et al* 2004, Menard *et al* 2011, 2010). However, conventional closed-bore scanners require to transfer the subject outside the bore during transperineal needle insertion, as there is limited access to the perineum due to the constrained in-bore space. Thus, there is no visual feedback during needle insertion, which is further complicated by the repeated patient transfer during a procedure. Recent advancements in magnet technologies have allowed

scanner manufacturers to design high-field closed-bore magnets with wider (70 cm) and shorter gantries that provide better access to the patient's perineum with superior image quality. To the best of our knowledge, there has been no custom-designed in-bore setup or navigation software to facilitate MRI-guided manual prostate biopsy using the transperineal approach, except for computer-controlled robotic devices (Fischer *et al* 2008, Song *et al* 2012, van den Bosch *et al* 2010, Muntener *et al* 2008, Cunha *et al* 2010), which still require further investigations to be used safely and regularly without any help from robotic specialists.

Thus, we developed such an in-bore setup and software that enables transperineal prostate biopsy in a wide and closed-bore 3T MRI scanner with the patient in the lithotomy position. Our goal was to attain better control of the needle insertion and minimize the safety hazard or special perioperative arrangement to bring the patient in and out of scanner bore. We also developed planning and navigation software to obtain MRI from the scanner by online connection and perform target planning, template registration and monitoring of the needle placement. We tested the overall template registration and needle-placement accuracy in a pre-clinical phantom validation study, and subsequently applied our methodology to ten clinical cases.

2. Materials and methods

2.1. Prostate intervention table with needle-guiding template

We designed and built a prostate intervention tabletop setup with built-in leg supports to allow the subject to be positioned in the lithotomy position in the scanner (figure 1). The tabletop was specifically designed to fit in a wide-bore (70 cm diameter) MRI scanner (MAGNETOM Verio 3T, Siemens AG, Erlangen, Germany). The patient is placed in the feet-first position to keep the patients face on the front side of the scanner, allowing the anesthesiologist and the vital monitor device to stay on the same side throughout the procedure. With this arrangement, the radiologist stands at the bore entrance on the back side of the scanner to reach the perineum of the patient. The tabletop consists of base board, leg supports, a needle-guiding template and a Z-shaped calibration marker (Z-frame) (DiMaio *et al* 2007). The baseboard is a wooden or plastic plate designed to fit on the patient table of the MRI scanner. The leg holders, attached to the baseboard by adjustable attachment, keep the legs apart and raised. The height of the tabletop from the floor of the scanner room is 91 cm, while the distance between the edge of the tabletop and the perineum was 76 cm. This configuration allows the radiologist to easily reach the perineum from the edge of the tabletop at the entrance of the bore of the MRI scanner (figure 1).

The needle-guiding template, originally developed for prostate cancer brachytherapy, is an acrylic block with dimensions of $100 \times 120 \times 25$ mm^3 with a grid of 1.3 mm diameter holes spaced 5 mm apart. It is fixed in the middle of the prostate intervention table located between the patient's legs and secured close to the subjects perineum. The template is supported by a two-degree-of-freedom (2-DOF) adjustable holder, which allows movement of the template in craniocaudal and anteroposterior directions. The Z-frame is attached in a predefined position to the template and is detached after calibration.

2.2. Calibration of needle-guiding template by Z-frame registration

The template is calibrated to the MRI coordinate system by imaging the Z-frame affixed to the template. The Z-frame has seven rigid tubes with 7.5 mm inner diameters filled with a contrast agent (MR Spots, Beekley, Bristol, CT) placed on three adjacent faces of a 60 mm cube, thus forming a Z-shaped enhancement in the images. It is registered by digitizing the

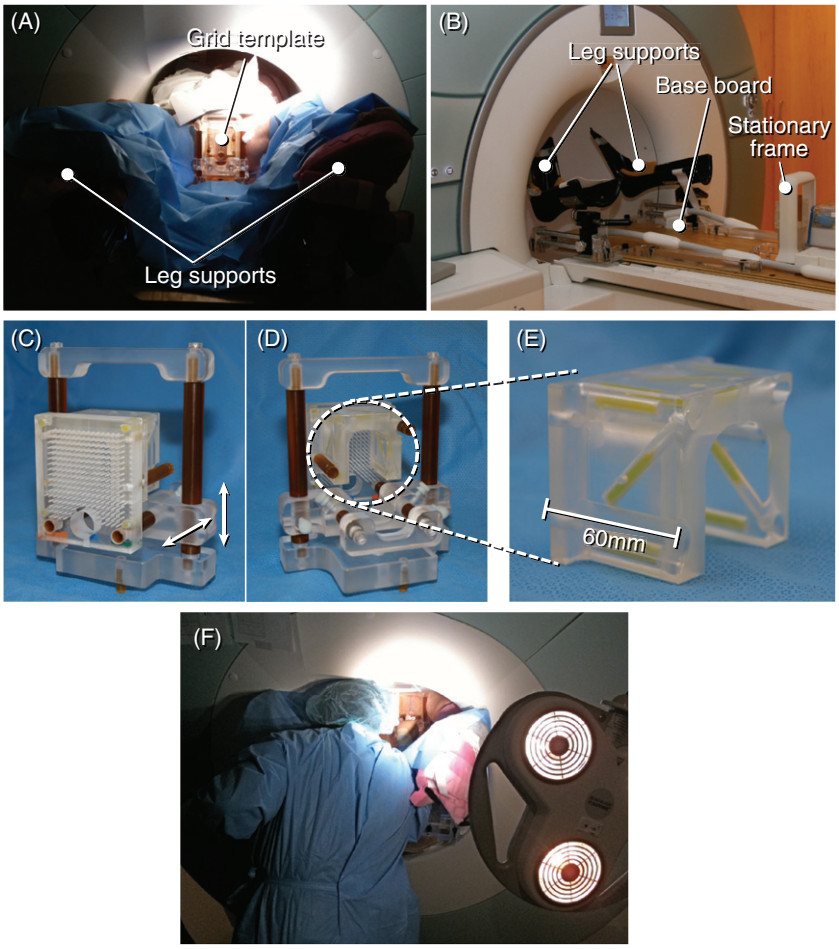

Figure 1. The photographs show (A) the overview of the prostate intervention table with leg supports during the clinical case, (B) the leg support, base board and stationary frame installed on the patient table of the scanner, (C, D) the front and rear view of the template with the Z-shaped calibration frame (Z-frame), (E) the close-up of the Z-frame and (F) the scene, where the radiologist was reaching the perineum during the procedure. The template is supported by a 2-DOF adjustable holder, which allows shifting the template in the craniocaudal (CC) and anteroposterior (AP) directions indicated by the arrows in (C).

hyper-intensity cross-section of the tubes in the marker to register the Z-frame to the MRI coordinate system. The seven rigid tubes are automatically detected on cross-sectional MRI images of the Z-frame, providing the location and orientation of the Z-frame in the MRI coordinate system (figure 2). We used the 3D fast low angle shot (FLASH) imaging sequence for calibration (TR/TE: 12 ms/1.97 ms; acquisition matrix: 256 × 256; flip angle 45°; field of view: 160 × 160 mm^2; slice thickness: 2 mm; receiver bandwidth: 400 Hz/pixel; number of averages: 3). The positions and orientations of the Z-frame calculated from the image slices that show the section of the seven rigid tubes were averaged. Once the Z-frame is registered to the MRI coordinate system, the geometric correlation between the template and the patient anatomy becomes known, enabling the selection of a hole that will guide a biopsy needle to a target previously defined by multi-parametric MR imaging. After the template is calibrated, the Z-frame is detached.

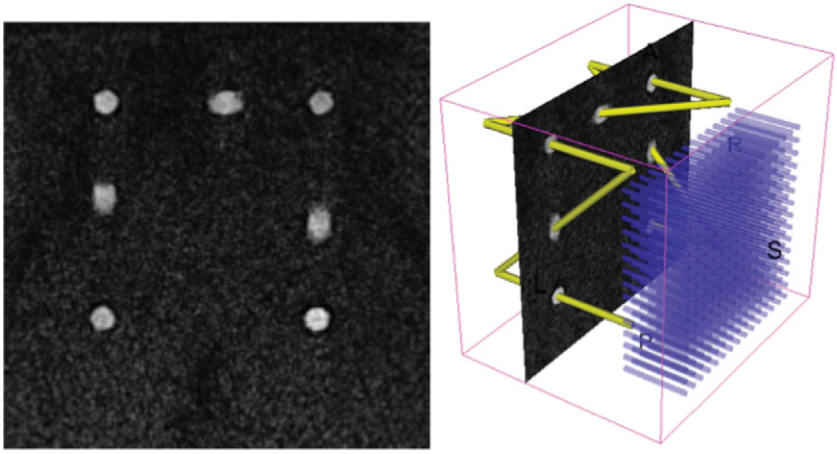

Figure 2. A 2D slice image of the Z-frame for the Z-frame registration (left) and the 3D view of the model of the Z-frame and the template overlaid on the slice image displayed on the navigation software. This 3D view representation allows the operator to visually confirm the result of the Z-frame registration intuitively.

2.3. Navigation software

We developed planning and navigation software for MRI-guided prostate biopsy as a plug-in software module for the open source medical image-processing and visualization software 3D slicer (http://www.slicer.org) (Gering *et al* 2001) to provide an integrated console to perform the following processes: (1) target planning based on preprocedural images, (2) image registration of preprocedural images and intraprocedural images, (3) needle-placement planning, (4) registration of the template using MR images of the Z-frame, (5) hole position calculation and (6) confirmation of needle placement. For image registration, we used B-spline non-rigid registration (Rueckert *et al* 1999) with maximization of mutual information (Mattes *et al* 2003) available as part of the BRAINSFit plug-in module (Johnson *et al* 2007) in 3D slicer. The image registration in process (2) also includes registration of planned targets defined on a preprocedural image prior to a procedure; the software applies a transformation that registers the preprocedural image to the intraprocedural image to map the target onto the intraprocedural image. In process (5), the hole positions and needle insertion depth for needle placement are calculated based on the target mapped onto the intraprocedural image, and the position and orientation of the template in the image coordinate system given by the template registration in process (4). For confirmation of needle placement in process (6), MR images of the placed needle is acquired and imported to the navigation software, where it is overlaid onto the intraprocedural image. The radiologist visually confirms the needle position and determines if reposition of the needle is necessary.

2.4. Preclinical validation studies

We conducted two phantom experiments in the wide-bore 3T MRI scanner to assess (1) the accuracy of Z-frame registration and (2) the overall accuracy of needle placement using a phantom. These studies investigated the feasibility of accurate needle placement using the template and Z-frame in a controlled environment.

Accuracy of Z-frame registration. We evaluated the translational registration error Δt and rotational registration error around the center of the Z-frame $\Delta\theta$ of the Z-frame registration. We also estimated the target registration error (TRE) to predict the largest possible targeting error of biopsy needle placement. The translational and rotational registration errors are defined as

$$\Delta t = t_I - t_P, \tag{1}$$

$$\Delta\theta = \arccos(R_I \boldsymbol{n} \cdot R_P \boldsymbol{n}), \tag{2}$$

where R_P and t_P are the physical rotation matrix and the physical translation vector of the Z-frame (gold standard), R_I and t_I are the rotation matrix and the translation vector of the Z-frame detected by the Z-frame registration method described above, n is a normal vector perpendicular to the axis of rotation R_P. The TRE is defined as the error between the needle tip position expected from the physical rotation and translation of the Z-frame and the needle tip position estimated from the rotation and translation of the Z-frame detected by the Z-frame registration method defined as

$$\mathrm{TRE} = (R_I \boldsymbol{v} + t_I) - (R_P \boldsymbol{v} + t_P), \tag{3}$$

where $\boldsymbol{v}$ is the translation vector representing the relative position of the needle tip with respect to the Z-frame coordinate system. In this study, R_P and t_P indicate the physical location of the Z-frame on the acrylic base with respect to the MR scanner. The acrylic base was first calibrated with the isocenter of the imaging bore using land-marking laser available in the scanner. The values of R_P and t_P were then found by aligning the Z-frame to the graduations printed on the acrylic base. The graduations allows the Z-frame to be placed at 0, 50, 100, 150 and 200 mm horizontally off the isocenter of the imaging bore, and tilted 0°, 5°, 10°, 15° and 20° horizontally from the main magnetic field. To evaluate the accuracy of Z-frame registration, while shifting the Z-frame along the Z-frames x- and y-axes and rotating around the Z-frames x-, y- and z-axes (roll, pitch and yaw, respectively), we placed the Z-frame on the acrylic base with respect to the MRI coordinate system as illustrated in figure 3. The shift along the z-axis, which corresponds to the SI axis in the MRI coordinate system, was not considered in this experiment, since the MRI scanner automatically positions the imaging subject to its isocenter by moving the table. Prior to shifting or rotating the Z-frame, the base with the graduation was calibrated in the MRI coordinate system by performing the Z-frame registration with placing the Z-frame at 0 mm off the center and 0° tilt from the main magnetic field. The amount of shifts along x- and y-axes and the roll, pitch and yaw rotations were varied independently to calculate Δt and $\Delta\theta$ using equation (1) and (2). For each shift and rotation, eight sets of 3D images of the Z-frame were acquired and processed to estimate the position and orientation of the Z-frame. The frequency and phase encoding directions were aligned to the x- and y-axes of the Z-frame, respectively, at the initial position (position and orientation before applying any shift or rotation) in order to simulate the image orientation in the clinical application, where the orientation of the Z-frame image is set to axial with respect to the patient (or MRI) coordinate system. A total of 240 images were acquired. In addition, the TRE was estimated assuming that the distance between the target and the center of the Z-frame was a needle length of 100 mm. In all measurements, average and standard deviation were computed and tabulated.

Accuracy of needle placement in the mock procedure. In our second experiment, we performed a second procedure using a prostate phantom (Model 053 Ultrasound Prostate Training Phantom, Computerized Imaging Reference Systems, Inc., Norfolk, VA) that mimics a gland, urethra, seminal vesicles and rectum on an MR image. The objective of this experiment

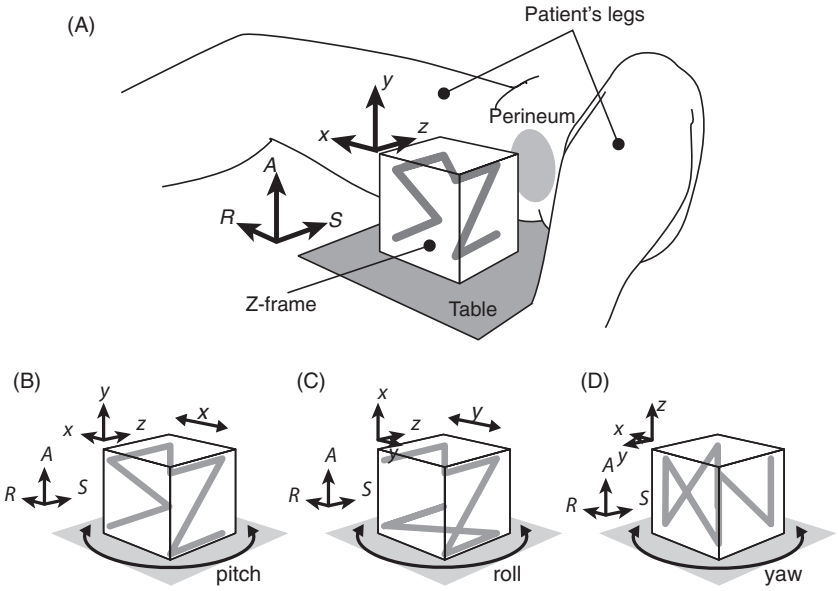

Figure 3. (A) The relationship between the Z-frame coordinate system (x, y, z) and the image coordinate system (R, A, S) in the clinical application is illustrated. The image coordinate system is defined, where the patient is positioned in feet-first, supine position in the magnet. To evaluate the accuracy of Z-frame registration, while shifting the Z-frame along the Z-frames x- and y-axes and rotated around the Z-frames$x$-, y- and z-axes (*roll*, *pitch* and *yaw*, respectively), the Z-frame on the acrylic base in three ways as illustrated above; the x-, y- and z-axes of the Z-frame were initially aligned to: (B) the RL-, AP- and SI-axes of the image coordinate system, respectively. to shift the Z-frame along the x-axis as well as rotate around the y-axis (pitch) of the Z-frame; (C) the AP-, RL- and SI-axes, respectively, to shift along the y-axis as well as to rotate around the x-axis (roll); (D) the RL-, SI- and AP-axes, respectively, to rotate around the z-axis (yaw).

was to evaluate the overall accuracy of needle placement in mock biopsy procedures in a controlled environment. The prostate phantom was placed in the magnet in a typical location of the prostate during a clinical procedure. The template with the Z-frame was fixed in front of the phantom so that the distance between the surface of the phantom and virtual targets defined in the phantom ranged from 60 to 120 mm. In each procedure, the image of the phantom and the Z-frame was acquired using a 3D FLASH sequence as described in the previous section, followed by the image of the phantom with a 2D turbo spin echo (TSE) sequence (TR/TE = 5250/100 ms; acquisition matrix = 320 × 224; flip angle = 150°; field of view = 160 × 160 mm^2; slice thickness = 3 mm; receiver bandwidth = 205 Hz/pixel). Those images were then loaded into 3D slicer to register the template to the MRI coordinate system and to define virtual targets in the prostate phantom. The virtual targets were randomly picked within each of eight segments in the mock prostate in the phantom, as indicated in figure 4. A total of eight virtual targets were defined for each procedure. 3D slicer determined the needle hole position and the insertion depth from the target positions. After a 18-gauge × 15 cm high-nickel-content stainless steel needle with diamond-shaped tip (MRI Bio Gun, E-Z-EM, Westbury, NY) was inserted, a confirmation image was acquired around the target with a half-Fourier acquisition single shot turbo spin echo (HASTE) sequence (TR/TE = 1000 ms/102 ms; matrix = 320 × 179; flip angle = 150°; field of view = 280 × 224 mm^2; slice thickness = 2 mm; receiver bandwidth = 780 Hz/pixel; acquisition time: 1 s) along the axial and the sagittal plane in order to measure the distance between the defined target and the center

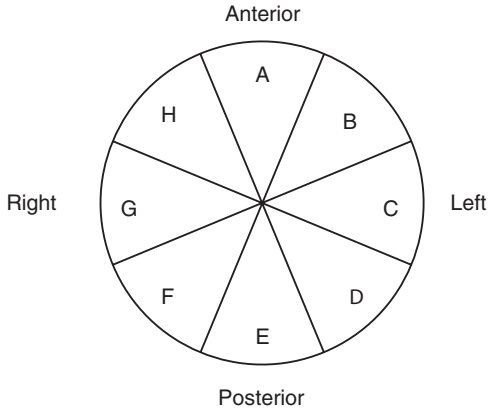

Figure 4. Eight targets were defined on the periphery of the mock prostate in the phantom. Each target was randomly picked up within each of segments A–H as indicated above. The diameter of the mock prostate was approximately 40 mm.

of the needle artifact on the same axial plane and to obtain 2D needle-placement error. The single shot turbo spine echo sequence was selected for this evaluation because our previous study demonstrated that the axis of the needle could accurately be localized by the artifact with an error of less than the level of pixel size (1 mm) when the needle was placed in parallel to the static field (DiMaio *et al* 2006). Four mock procedures were performed, resulting in a total of 32 biopsies in the study. Two types of error were evaluated retrospectively: *targeting error*, defined by the distance between the planned target position and the center of the needle artifact on the needle confirmation image; *needle-placement error*, defined by the distance between the 'expected needle position' and the center of the needle artifact. The expected needle position was the needle position reachable from the needle hole and needle insertion depth determined by 3D slicer. Therefore, the difference between the targeting error and the needle-placement error is whether they take into account the effect of the 5 mm gap between the holes on the template. 2D root mean square (RMS) of both targeting error and needle-placement error was computed for each segment in figure 4, as well as for all 32 biopsies.

2.5. Clinical studies

We conducted an investigation during initial clinical studies to assess the safety and feasibility of the methods developed. Ten men (age range: 50–73 years; weight range: 147–211 lbs) underwent targeted core biopsy of the prostate in the wide-bore 3T MRI scanner. The study protocol was approved by the Brigham and Womens Hospitals Institutional Review Board prior to patient enrollment and was HIPAA compliant. The patients with suspicious foci were eligible for the study after undergoing a multi-parametric 3T MRI examination with endorectal coil. All patients had elevated serum prostate specific antigen (PSA) and a dominant index lesion (most suspicious for cancer) on recent diagnostic 3T prostate MRI. Index lesions were depicted as a focus of decreased T2 signal on T2-weighted imaging (T2WI), restricted diffusion on diffusion weighted imaging (DWI), and early arterial phase enhancement with rapid wash-out on dynamic contrast enhanced (DCE) sequences. Clinical indications included: inability to obtain TRUS-guided biopsy due to total colectomy ($N = 1$) or inflamed ileal J-pouch ($N = 1$), multiple prior negative TRUS-guided biopsies ($N = 6$), prior prostate brachytherapy and MRI focus suspicious for recurrence ($N = 1$), and MRI focus suspicious for higher

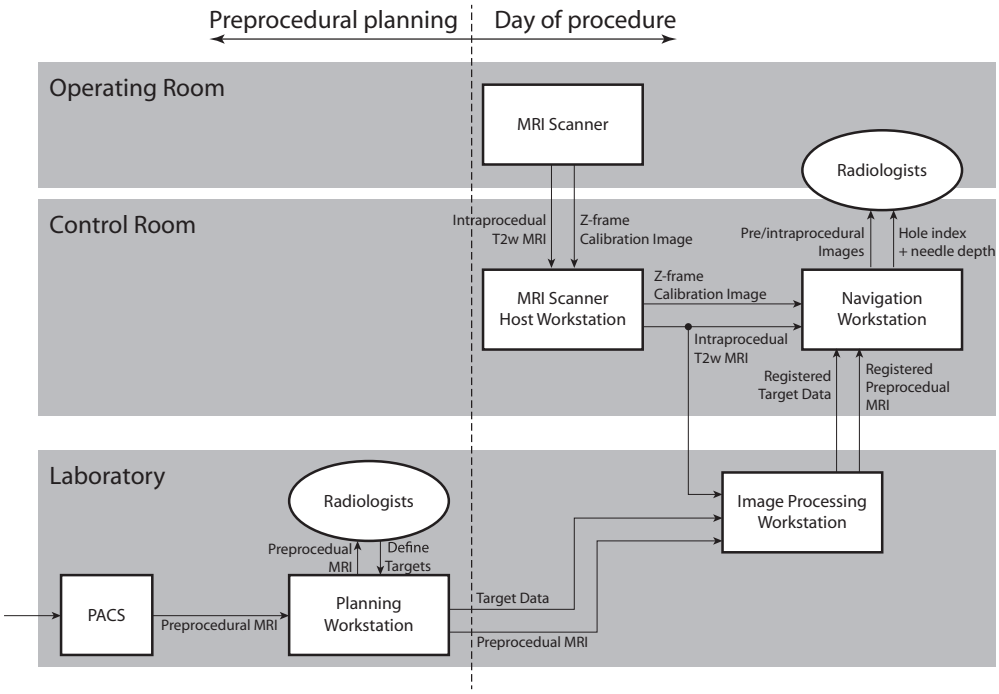

Figure 5. The system configuration and the data flow before and during the procedure is shown. For preprocedural planning, which took place a few days before the procedure, preprocedural MRI data, including T2W, DCE, and diffusion-weighted images were retrieved from the hospitals picture archiving and communication system (PACS). The radiologists identified the suspicious foci as biopsy targets based on the preprocedural MRI. During the procedure, intraprocedural T2W MRI acquired by the MRI scanner in the operating room was transferred from the host workstation to the navigation workstation for intraprocedural planning and the image-processing workstation for registering the preprocedural MRI and the biopsy targets to the intraprocedural MRI. The registered preprocedural MRI and registered targets were returned to the navigation workstation for the radiologists review and calculation of the template hole index and depth for guiding the needle.

grade tumor than suggested at prior TRUS-guided biopsy ($N = 1$). Informed consent for the procedure was obtained from each subject after the nature of the procedure and the potential hazards had been fully explained. The system configuration and flow of data before and during the procedure are shown in figure 5. The workflow of the procedure was as follows.

- *Preprocedural planning.* Two radiologists reviewed preprocedural multi-parametric MRI exams, consisting of T2-weighted MRI, pharmacokinetic parameter maps obtained from DCE-MRI, and apparent diffusion coefficient (ADC) maps calculated from diffusion-weighted MRI, to identify suspicious targets. These preprocedural images and the preprocedural targets were stored in the image-processing workstation for intraprocedural image registration.
- *Patient preparation.* On the day of the biopsy, the patient was taken to the 3T MRI with a 70 cm wide-bore (MAGNETOM Verio 3T, Siemens AG, Erlangen, Germany) and placed supine on the prostate intervention table in feet-first orientation so that the radiologist could approach the perineum from the other side of the magnet. The leg supports were adjusted and fixed, the patient was positioned in the lithotomy position, and the imaging

coil (Body Matrix Coil, Siemens AG, Erlangen, Germany) was placed over the anterior lower pelvis on the front side of the scanner. The patient was then transferred to the other side of the magnet in the far end of the room, where the perineum was prepped and draped in a sterile fashion. The sterile stationary frame and the template with the Z-frame were set up. When the radiologist confirmed that all instruments were properly adjusted, the patient was moved into the isocenter of the magnet for imaging. The procedures were performed under standard departmental guidelines using intravenous conscious sedation (typically using Versed and Fentanyl).

- *Pre-procedural MRI and planning in 3D slicer.* Two sets of MR images were acquired after the patient was positioned in the isocenter of the magnet. The first was a 3D image of the Z-frame acquired by a 3D FLASH sequence with the same parameters used in the preclinical study. The Z-frame image was transferred to the navigation workstation for localization of the Z-frame as described above. The second image was an intraprocedural 2D multi-slice T2-weighted (T2W) image of the prostate acquired by TSE sequence with the same parameters as the preclinical study. The intraprocedural T2W image was acquired while the Z-frame was being localized on the navigation workstation. The intraprocedural T2W prostate image was transferred to the navigation workstation, where the radiologist identified suspicious foci shown in the T2 image as intraprocedural targets. While the radiologist was reviewing the intraprocedural T2W prostate image, the image was also transferred to the image-processing workstation in order to register the preprocedural T2W image to the intraprocedural T2 image using the B-spline deformable image registration (Oguro *et al* 2009, Fedorov *et al* 2012). Including manual cropping of the region of interest, it took 5–10 min to register the preprocedural T2W image to the intraprocedural T2W image. The detail of the deformable image registration methodology is described in our separate report (Fedorov *et al* 2012). The planning and registration processes were performed in parallel to minimize time. The transformation derived from the deformable image registration was then used to register the preprocedural targets to the intraprocedural T2W MRI. Once all the intraprocedural targets and preprocedural targets were projected on the intraprocedural T2W image, 3D slicer selected the optimal template holes for inserting the biopsy needle and the insertion depth of the needles.
- *Needle placement and monitoring.* After the Z-frame was detached from the template, the radiologist first applied local anesthetic and then inserted an 18-gauge $\times$ 15 cm MRI-compatible core biopsy needle (one of the following three types: MRI Bio Gun, E-Z-EM, Westbury, NY; Single Action Biopsy Device, US Biopsy, Franklin, IN; Semi Automatic Biopsy Gun, Invivo, Schwerin, Germany; Fully Automatic Biopsy Gun, Invivo, Schwerin, Germany) through the selected hole until it reached the calculated insertion depth. The depth of the needle insertion was previously marked on the outer shaft of the needles by the radiologist. Once the needle was inserted, a 2D needle confirmation image was obtained in either the axial or the coronal plane at the planned target position using either 2D Turbo FLASH sequence (TR/TE = 402.21 ms/1.45 ms; acquisition matrix = 128 $\times$ 115; flip angle = 140°; field of view = 200 $\times$ 200 mm^2; slice thickness = 3 mm; receiver bandwidth = 1500 Hz/pixel; imaging time: 400 ms) (cases 1–8) or 2D multislice TSE (TR/TE = 2700 ms/106 ms; acquisition matrix = 280 $\times$ 280; flip angle = 48°; field of view = 200 $\times$ 200 mm^2; slice thickness = 3 mm; receiver bandwidth = 252 Hz/pixel; imaging time: approx. 1 min) (cases 9, 10) to confirm that the needle was placed at the desired position. If the needle was not found to be close enough to the target lesion, the needle was reinserted through an alternative hole selected based on MR image guidance. Upon satisfactory placement of the needle tip over the target based upon MR, the tissue samples were collected, labeled and sent for site-specific pathological examination.

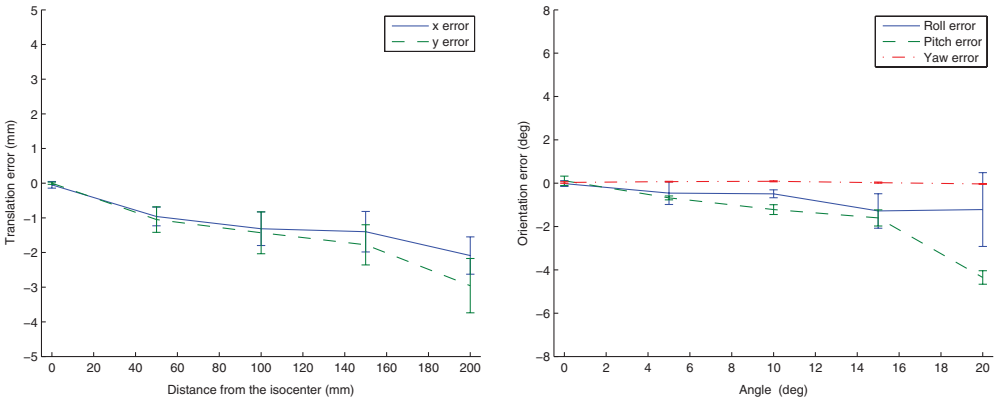

Figure 6. The translational and rotational registration errors in Z-frame registration, when the Z-frame was placed at 0, 50, 100, 150, and 200 mm horizontally off the isocenter along the x- and y-axes of the Z-frame, and tilted 0°, 5°, 10°, 15° and 20° in roll, pitch and yaw of the Z-frame ($N = 8$).

- *Evaluation of needle placement accuracy.* The *targeting error* and the *needle placement error* (see the section *Accuracy of needle placement in the mock procedure* for definitions) were retrospectively measured to investigate the needle-placement precision, which can vary due to the 5 mm gap between needle insertion holes. Since the core biopsy needle cuts a 20 mm length of tissue along the needle axis, the accuracy of needle placement was evaluated within the axial plane, which is approximately perpendicular to the needle. The average and standard deviation of placement accuracy were computed as RMS from all needle insertion trials and were tabulated. In addition, as secondary measurements, numbers of target sites and time taken per procedure were recorded and averages were tabulated.

3. Results

3.1. Preclinical validation studies

The translational registration error along the x- and y-axes and the rotational registration error in roll, pitch and yaw are shown in figure 6; the overall translational errors were -1.1 ± 0.8 mm for the x-direction and -1.4 ± 1.1 mm for the y-direction corresponding to RL and AP directions of the patient, respectively (see figure 6). The rotational errors were $(0.8 \pm 1.0)^\circ$ in roll, $(-1.7 \pm 1.6)^\circ$ in pitch and $(0.0 \pm 0.0)^\circ$ in yaw, corresponding to the rotations around RL-, AP- and SI-axes in the clinical setting. The expected TRE for a 100 mm needle are shown in figure 7. In the mock procedure, the RMS targeting error was 3.0 mm, while the RMS needle-placement error was 2.4 mm. The relationship between the targeting error and the location of the target in the prostate in the mock procedure is shown in figure 8.

3.2. Clinical study

All ten procedures were technically successful and patients tolerated the procedure well without intraprocedural or postprocedural pain. Table 1 summarizes the needle-placement accuracy per case. Two patients had asymptomatic self-limited small periprostatic hematoma on imaging. No other complications were encountered. For each patient, two–five targets were

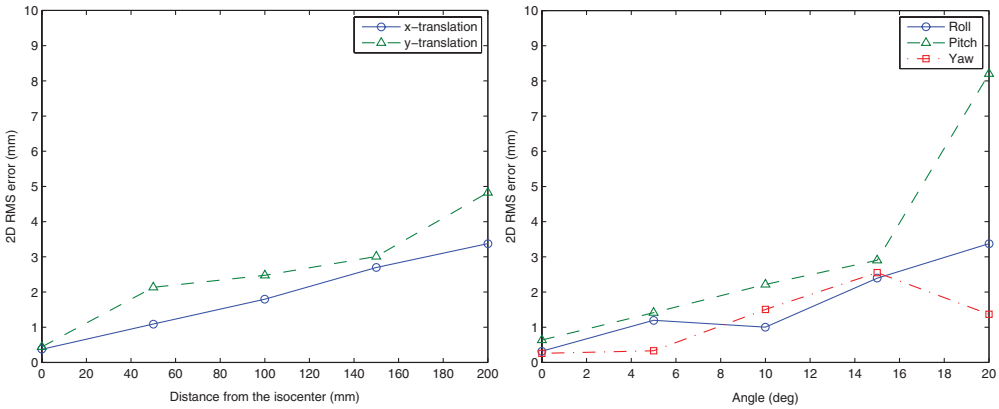

Figure 7. The 2D expected TRE of Z-frame registration for a 100 mm needle are shown. For the left graph, the Z-frame was placed at 0, 50, 100, 150 and 200 mm off center in the *x*- and *y*-directions ($N = 4$ for each distance), while the orientation of the Z-frame was fixed to the original direction (no tilt in any direction). For the right graph, the Z-frame was tilted 0°, 5°, 10°, 15° and 20° in roll, pitch and yaw of the Z-frame ($N = 8$), while the center of the Z-frame was fixed at the isocenter. In this evaluation, all translational and rotational errors were taken into account.

Table 1. The results of needle placement in the ten clinical cases including the number of targets, the targeting error, the needle-placement error are shown. All errors were measured in the 2D axial plane at the planned target and shown as RMS errors. The 2D RMS targeting error and needle-placement error through the ten cases were 5.4, and 5.7 mm respectively.

Case	Number of targets	Targeting error (mm)	Needle placement error (mm)	Duration (min)
1	2	5.4	8.4	105
2	3	4.5	4.1	100
3	5	3.3	4.2	110
4	5	7.6	7.4	90
5	6	3.5	3.6	130
6	4	8.5	9.1	105
7	5	2.9	2.9	105
8	4	6.1	6.7	65
9	2	4.4	3.3	110
10	4	5.6	4.8	120

identified on pre-biopsy MR images and selected for biopsy. MR images from a clinical case are shown in figure 9. Despite the lack of an endorectal coil, the images provide sufficient contrast of the prostate and its substructures, allowing us to perform automatic deformable registration of the preprocedural and intraprocedural MRI with acceptable accuracy, reliability and computation time (Fedorov *et al* 2012). The quality of tissue core samples was acceptable by visual observation during the procedure. Tissues were sampled from an average of four locations in 104 min per procedure. The 2D RMS targeting error was 5.4 mm, while the RMS needle-placement error was 5.7 mm. The duration of the procedures ranged from 65 to 130 min including 25–70 min of preparation, e.g., patient setup and coil placement. In some studies, such as case 5, movement of the patients led to repositioning of the template and the coil, prolonging the time for setup.

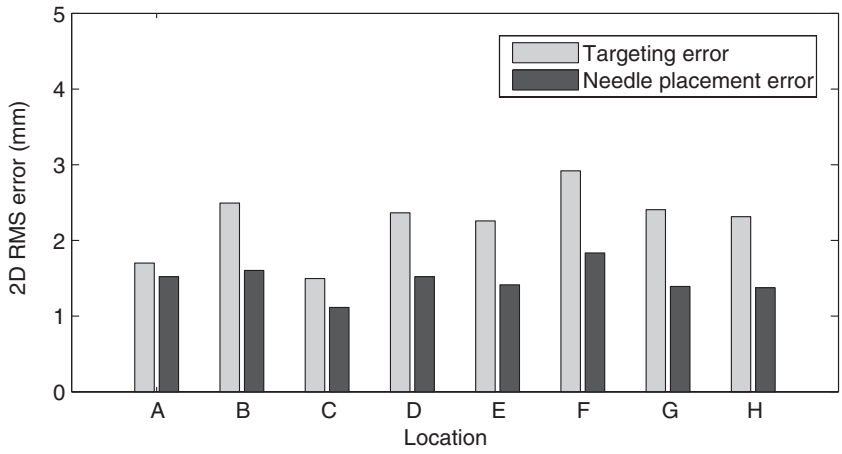

Figure 8. The relationship between the 2D RMS errors of the needle placement and each target area in the prostate phantom. Labels A–H on the graph correspond to the labels defined in figure 4.

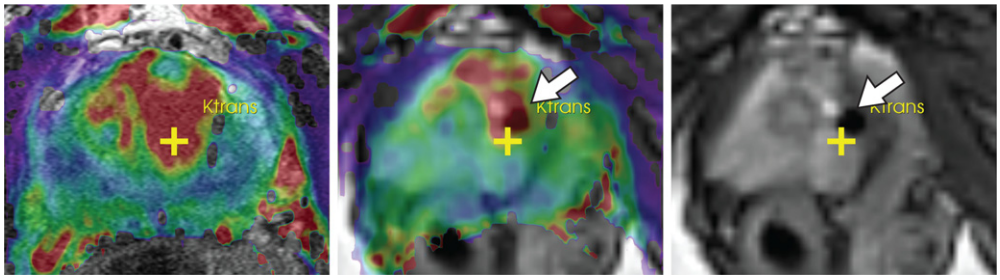

Figure 9. Example MR images from one clinical case. A target point was defined within the central gland with a high value in the K^{trans} pharmacokinetic parameter map registered and overlaid on the intraprocedural T2w image (left). The needle placement was confirmed by the artifact shown on the real-time TurboFLASH MR image (indicated in the middle and right images).

4. Discussion

We have developed and report here a prostate intervention apparatus and compatible software to support transperineal manual needle placement into the prostate in a wide-bore 3T MRI scanner. The in-bore tabletop setup and software can also be used for prostate therapy techniques, such as brachytherapy, laser ablation, or cryoablation, since these therapies are performed using the transperineal approach rather than transrectal. We performed both a phantom study to investigate the accuracy of needle placement and a preliminary clinical study to assess the accuracy, safety and feasibility of the procedure, the equipment and software. The contributions of this paper are the novel engineering solutions that allow us to perform accurate core needle prostate biopsy, and accuracy assessment of template registration and needle placement in both phantom and patients. To the best of our knowledge, only a limited number of previous studies have assessed the needle-placement accuracy for MRI-guided transperineal template biopsy and interventions in patients (Susil *et al* 2004, Blumenfeld *et al* 2007, Menard *et al* 2010), animal (Lakosi *et al* 2009) and cadavers (Woodrum *et al* 2010), and none of them have performed comprehensive accuracy evaluation including

calibration of guidance tools and needle placement in phantoms and patients, except the work of Blumenfeld *et al* (2007). It would also be desirable to further investigate other source of errors, e.g., geometric accuracy of the MRI scanner, tissue deformation and needle deflection for this particular application.

One of the important benefits of intraprocedural 3T MRI is its superior image quality, which is ideal for accurate fusion of preprocedural diagnostic MRI and intraprocedural guidance image. Mapping preprocedural MRI onto the guidance image has been of major clinical interest; several groups have demonstrated image fusion of preprocedural diagnostic MRI with intraprocedural TRUS (Ukimura *et al* 2010, Natarajan *et al* 2011) or intraprocedural MRI (Hambrock *et al* 2008, Franiel *et al* 2011). While these investigators have used rigid registration (Ukimura *et al* 2010), surface shape (Natarajan *et al* 2011) or visual assessment (Hambrock *et al* 2008, Franiel *et al* 2011), our study demonstrated that automatic deformable registration is indeed feasible for pre- and intraprocedural MRI fusion. We have reported the detail of our intraprocedural automated deformable image registration methodology with an average in-slice landmark registration error of 1.3 ± 0.5 mm and computation time of at most 2 min (Fedorov *et al* 2012). Mapping preprocedural MRI onto guidance images is desirable even for a procedure guided by such state-of-the-art 3T MRI, because often it is not practical to perform multiparametric MRI study and MRI-guided biopsy in the same imaging session due to time constraints. This outcome leads us to believe that our method allows for a precise site-specific pathological correlation with MR image abnormalities. This feature is critical for providing tissue validation of the pre-biopsy MR image parameters; this would only be available otherwise through radical prostatectomy, with image registered to whole-mount pathology of the gland specimen. This analysis is not easily obtained and certainly not available in all men as they do not all undergo surgery.

The accuracy study on Z-frame registration showed that the translational error of the Z-frame registration was 1.4 mm along the axis plane, and 0.8° maximum in axial plane rotation, which are comparable to other studies using fiducials for calibration (Dumoulin *et al* 1993, Engelhard *et al* 2006, Patil *et al* 2009, Rea *et al* 2008). There are several factors that may affect the accuracy of the Z-frame registration. First, a degraded signal-to-noise ratio due to the selection of the coil may affect the accuracy of Z-frame registration; our previous study of Z-frame registration using a head coil (DiMaio *et al* 2007) showed better registration accuracy than this study probably due to the better signal-to-noise ratio of the head coil. In this study, the body matrix coils were used in a 3T scanner to cover both the pelvic area and the Z-frame in the clinical setting. It is of our interest to assess the impact of image quality on the accuracy of registration in the future. Second, the geometric accuracy of images from the wide- and short-bore MRI scanner due to the field inhomogeneity is another possible source of the Z-frame registration error. Although further investigation is required to quantify it, our result (figure 6) suggests that it is not a major concern in our clinical application, because the translational error of the Z-frame registration did not change dramatically within 15 cm from the isocenter, which covers the typical positions of the Z-frame and the area of the prostate gland. Third, the rotational error also depends on the orientation of the rotation; the error in the rotation around the SI-axis was significantly smaller than the errors for the other axes. This can be explained by the fact that the rotation around the SI-axis is in-plane with respect to the slice of the Z-frame images, while the others are out-of-plane. If θ and d are the rotational angle and the size of the Z-frame cube, respectively, the in-plane rotation is associated with the shift of the bright spots proportional to $\theta d/2$ on the Z-frame image, while the out-of-plane rotations are associated with the change of the distances between the bright spots proportional to $d(1 - \cos(\theta))/2$. Consequently, in-plane motion causes larger shift of the bright spots on the image when θ is sufficiently small. Adding diagonal tubes on the superior and inferior

faces of the cube and acquiring images in the three orthogonal planes would help improve the rotational accuracy of the Z-frame registration. Fourth, the limited length of the tubes filled with the contrast agent attached to the Z-frame limits the range of tilting angle that is accurately detected by the Z-frame registration. Because we chose to use the commercially available approved makers to build our Z-frame with the scope of the clinical application, the tube was not sufficiently long for the diagonal rod of the Z-frame; it was difficult to maintain all three diagonal tubes within the axial imaging plane, especially when the Z-frame was rotated around the y-axis (or in pitch) by a large angle. This may explain why we observed a larger error in rotations in pitch than that in roll and yaw.

In our mock procedures, we found that the RMS targeting error was 3.0 mm, while the RMS needle-placement error was 2.4 mm. This indicates that the inaccuracy of needle targeting was caused primarily by Z-frame registration and needle deflection (2.4 mm), while the error due to the limited number of needle insertion holes is less. The RMS error expected from the Z-frame registration error was within 2.5 mm, while the Z-frame was less than 100 mm from the isocenter (figure 7); this result suggests that the needle deflection contributed to the targeting error. This result is comparable to our previous study (Blumenfeld *et al* 2007), where the template registration error was responsible for 1.5 ± 0.3 mm of needle-placement error and needle deflection was responsible for $0.6 - 1.1$ mm of placement error.

Our clinical study shows that the technique is feasible in its ability to approach the prostate gland transperineally in a 3T scanner, utilizing the lithotomy position while keeping the patient inside the magnet for repeated imaging. It allows needle placement with 5.4 mm accuracy in clinical biopsies, which was superior to our previous clinical study using 18-gauge needle in the 0.5 T MRI scanner, where the targeted biopsy error was 6.5 ± 3.5 (Blumenfeld *et al* 2007). The larger error in clinical studies than that in the phantom study is typically due to the *in vivo* conditions, e.g., patient tissue motion, tissue interfaces, which can displace the needle. In some cases pubic bones can also cause increased needle deflection. The result was also comparable to the needle-placement error in clinical studies on transrectal needle placement; Engelhard *et al* (2006) reported that the needle was successfully placed in suspected lesion less than 10 mm; Schouten *et al* (2012) compared their robotic device for transrectal biopsies and commercially available transrectal biopsy device in 13 clinical biopsy procedures resulting mean targeting error of 5.7 and 5.8 mm, respectively. However, our needle placement was not as accurate as the studies using thicker needles; Susil *et al* (2004) reported that the needle-placement accuracy was 2.1 mm in eight clinical transperineal high-dose-rate brachytherapy studies using a 14-gauge needle guided by 1.5 T MRI scanner; Woodrum *et al* (2010) demonstrated needle placement for transperineal laser ablation under a 3.0 T MRI scanner using a 14-gauge needle with the needle-placement error of 2.1 mm in their cadaveric study. This indicates that the deflection of the biopsy needle is a major concern in accurate needle placement.

The study also serves as an important engineering step toward clinical application of MRI-guided robotic transperineal prostate interventions, which is expected to improve ergonomics and accuracy in needle placement (Fischer *et al* 2008, Song *et al* 2012, Seifabadi *et al* 2012). We are currently developing an MRI-compatible needle-placement robot that works with the presented in-bore setup and the navigation software. The robot will be built into the clinical workflow, imaging, software operation and needle placement, which have been developed and proven clinically feasible in this study. Several groups have already demonstrated that remotely controlled MRI-compatible needle-placement robots improve the ergonomics of the operation. Muntener *et al* (2008) and Cunha *et al* (2010) developed a fully-automated needle-placement robot for seed delivery in brachytherapy, which does not require a radiologist to reach to the perineum in the closed in-bore space for manipulation of the needle. Recently, Yakar *et al*

(2011) and Schouten *et al* (2012), and Zangos *et al* (2011) demonstrated clinical application of remotely controlled MRI-compatible robots for positioning of needle guides in transrectal and transgluteal biopsies, respectively. These robots allow positioning and orienting the needle guides in the scanners remotely with real-time MRI guidance, making the targeting process ergonomically comfortable for operating physicians. The advantage of robotic operation over manual operation in terms of targeting accuracy has not been proven in the clinical trials yet (Schouten *et al* 2012). However, robots allows unique mechanical motion such as step-wise tapping of needles to reduce tissue dragging, potentially improving the needle-placement accuracy (van den Bosch *et al* 2010).

The limitation of this study is that we only considered geometrical error of needle placement by comparing the distance between the planned target and the actual needle position estimated from the confirmation image. A more complete analysis of clinical outcome should also take into account the inaccuracy due to misalignment secondary to prostate motion voluntary and involuntary between the preprocedural diagnostic image and intraprocedural image, and the deformation and displacement of the prostate gland during the biopsy procedure, which will be evaluated in future work.

In conclusion, we developed a prostate intervention table and software that support transperineal manual needle biopsies in a wide-bore 3T MRI scanner. The table is equipped with a template with a Z-shaped calibration frame that allows needle placement with an error of 5.4 mm in clinical biopsies. Our preclinical and early clinical studies have shown the technique to be feasible, given that the targeting error was comparable to the clinical studies in the literature. This approach allows for the site-specific pathological tissue analysis of focal MRI-detected abnormalities in the prostate gland.

Acknowledgments

This work was supported by National Institute of Health (1R01CA111 288, 5P01CA067 165, 5P41RR019 703, P41EB015 898, R01CA124 377, 1R01CA138 586, 5U54EB005 149), Center for Integration of Medicine and Innovative Technology (CIMIT 11-325), Siemens/Brigham and Women's Hospital (BWH) Seed Grant Award, and Intelligent Surgical Instruments Project of METI, Japan. The content of this paper is solely the responsibility of the authors and does not necessarily represent the official views of the NIH. We thank Janice Fairhurst, Nancy Trane, Colleen Huether and Daniel Kacher of BWH for their technical support, and Angela Roddy Kanan of BWH for her clinical support.

References

Beyersdorff D, Taupitz M, Winkelmann B, Fischer T, Lenk S, Loening S A and Hamm B 2002 Patients with a history of elevated prostate-specific antigen levels and negative transrectal US-guided quadrant or sextant biopsy results: value of MR imaging *Radiology* **224** 701–6

Blumenfeld P, Hata N, DiMaio S, Zou K, Haker S, Fichtinger G and Tempany C M 2007 Transperineal prostate biopsy under magnetic resonance image guidance: a needle placement accuracy study *J. Magn. Reson. Imaging* **26** 688–94

Cormack R A, D'Amico A V, Hata N, Silverman S, Weinstein M and Tempany C M 2000 Feasibility of transperineal prostate biopsy under interventional magnetic resonance guidance *Urology* **56** 663–4

Cunha J A, Hsu I C, Pouliot J, Roach I M, Shinohara K, Kurhanewicz J, Reed G and Stoianovici D 2010 Toward adaptive stereotactic robotic brachytherapy for prostate cancer: demonstration of an adaptive workflow incorporating inverse planning and an MR stealth robot *Minim. Invasive Ther. Allied Technol.* **19** 189–202

D'Amico A V, Tempany C M, Cormack R, Hata N, Jinzaki M, Tuncali K, Weinstein M and Richie J P 2000 Transperineal magnetic resonance image guided prostate biopsy *J. Urol.* **164** 385–7

de Oliveira A, Rauschenberg J, Beyersdorff D, Semmler W and Bock M 2008 Automatic passive tracking of an endorectal prostate biopsy device using phase-only cross-correlation *Magn. Reson. Med.* **59** 1043–50

DiMaio S P, Kacher D F, Ellis R E, Fichtinger G, Hata N, Zientara G P, Panych L P, Kikinis R and Jolesz F A 2006 Needle artifact localization in 3T MR images *Stud. Health Technol. Inform.* **119** 120–5 PMID: 16404029

DiMaio S P, Samset E, Fischer G, Iordachita I, Fichtinger G, Jolesz F and Tempany C M 2007 Dynamic MRI scan plane control for passive tracking of instruments and devices *Lect. Notes Comput. Sci.* **4792** 50–8

Dumoulin C L, Souza S P and Darrow R D 1993 Real-time position monitoring of invasive devices using magnetic resonance *Magn. Reson. Med.* **29** 411–5

Engelhard K, Hollenbach H P, Kiefer B, Winkel A, Goeb K and Engehausen D 2006 Prostate biopsy in the supine position in a standard 1.5-T scanner under real time MR-imaging control using a MR-compatible endorectal biopsy device *Eur. Radiol.* **16** 1237–43

Fedorov A, Tuncali K, Fennessy F M, Tokuda J, Hata N, Wells W M, Kikinis R and Tempany C M 2012 Image registration for targeted MRI-guided transperineal prostate biopsy *J. Magn. Reson. Imaging* (available online, doi:10.1002/jmri.23688)

Fischer G S, Iordachita I, Csoma C, Tokuda J, DiMaio S P, Tempany C M, Hata N and Fichtinger G 2008 MRI-compatible pneumatic robot for transperineal prostate needle placement *IEEE/ASME Trans. Mechatronics* **13** 295–305

Franiel T, Stephan C, Erbersdobler A, Dietz E, Maxeiner A, Hell N, Huppertz A, Miller K, Strecker R and Hamm B 2011 Areas suspicious for prostate cancer: MR-guided biopsy in patients with at least one transrectal US-guided biopsy with a negative finding—multiparametric MR imaging for detection and biopsy planning *Radiology* **259** 162–72

Gering D T *et al* 2001 An integrated visualization system for surgical planning and guidance using image fusion and an open MR *J. Magn. Reson. Imaging* **13** 967–75

Hambrock T, Futterer J J, Huisman H J, Hulsbergen-vandeKaa C, van Basten J P, van Oort I, Witjes J A and Barentsz J O 2008 Thirty-two-channel coil 3 T magnetic resonance-guided biopsies of prostate tumor suspicious regions identified on multimodality 3 T magnetic resonance imaging: technique and feasibility *Invest. Radiol.* **43** 686–94

Hata N *et al* 2001 MR imaging-guided prostate biopsy with surgical navigation software: device validation and feasibility *Radiology* **220** 263–8 (available at http://radiology.rsna.org/content/220/1/263.long)

Hodge K K, McNeal J E, Terris M K and Stamey T A 1989 Random systematic versus directed ultrasound guided transrectal core biopsies of the prostate *J. Urol.* **142** 71–4 (discussion 74–5)

Johnson H, Harris G and Williams K 2007 BRAINSFit: mutual information registrations of whole-brain 3D images, using the Insight Toolkit *Insight J.* (http://hdl.handle.net/1926/1291)

Krieger A, Susil R C, Menard C, Coleman J A, Fichtinger G, Atalar E and Whitcomb L L 2005 Design of a novel MRI compatible manipulator for image guided prostate interventions *IEEE Trans. Biomed. Eng.* **52** 306–13

Lakosi F, Antal G, Vandulek C, Kovacs A, Garamvolgyi R, Petnehazy O, Bajzik G, Hadjiev J, Repa I and Bogner P 2009 Technical feasibility of transperineal MR-guided prostate interventions in a low-field open MRI unit: canine study *Pathol. Oncol. Res.* **15** 315–22

Mattes D, Haynor D R, Vesselle H, Lewellen T K and Eubank W 2003 PET-CT image registration in the chest using free-form deformations *IEEE Trans. Med. Imaging* **22** 120–8

Menard C *et al* 2004 MRI-guided HDR prostate brachytherapy in standard 1.5 T scanner *Int. J. Radiat. Oncol. Biol. Phys.* **59** 1414–23

Menard C *et al* 2010 Online guidance of tumor targeted prostate brachytherapy using histologically referenced MRI *18th Scientific Meeting and Exhibition of International Society of Magnetic Resonance in Medicine* vol 18 p 6693

Menard C *et al* 2011 MRI and biopsy performance in delineating recurrent tumor boundaries after radiotherapy for prostate cancer *19th Scientific Meeting and Exhibition of International Society of Magnetic Resonance in Medicine* vol 19 p 3072

Muntener M, Patriciu A, Petrisor D, Schr M, Ursu D, Song D Y and Stoianovici D 2008 Transperineal prostate intervention: robot for fully automated MR imaging–system description and proof of principle in a canine model *Radiology* **247** 543–9

Natarajan S, Marks L S, Margolis D J, Huang J, Macairan M L, Lieu P and Fenster A 2011 Clinical application of a 3D ultrasound-guided prostate biopsy system *Urol. Oncol.* **29** 334–42

Oguro S, Tokuda J, Elhawary H, Haker S, Kikinis R, Tempany C M and Hata N 2009 MRI signal intensity based b-spline nonrigid registration for pre- and intraoperative imaging during prostate brachytherapy *J. Magn. Reson. Imaging.* **30** 1052–8

Patil S, Bieri O, Jhooti P and Scheffler K 2009 Automatic slice positioning (ASP) for passive real-time tracking of interventional devices using projection-reconstruction imaging with echo-dephasing (PRIDE) *Magn. Reson. Med.* **62** 935–42

Presti J J C, Chang J J, Bhargava V and Shinohara K 2000 The optimal systematic prostate biopsy scheme should include 8 rather than 6 biopsies: results of a prospective clinical trial *J. Urol.* **163** 163–6

Presti J J C, O'Dowd G J, Miller M C, Mattu R and Veltri R W 2003 Extended peripheral zone biopsy schemes increase cancer detection rates and minimize variance in prostate specific antigen and age related cancer rates: results of a community multi-practice study *J. Urol.* **169** 125–9

Rea M, McRobbie D, Elhawary H, Tse Z T H, Lamperth M and Young I 2008 System for 3-D real-time tracking of MRI-compatible devices by image processing *IEEE/ASME Trans. Mechatronics* **13** 379–82

Roehl K A, Antenor J A and Catalona W J 2002 Serial biopsy results in prostate cancer screening study *J. Urol.* **167** 2435–9

Rueckert D, Sonoda L I, Hayes C, Hill D L G, Leach M O and Hawkes D J 1999 Nonrigid registration using free-form deformations: application to breast MR images *IEEE Trans. Med. Imaging* **18** 712–21

Sartor A O, Hricak H, Wheeler T M, Coleman J, Penson D F, Carroll P R, Rubin M A and Scardino P T 2008 Evaluating localized prostate cancer and identifying candidates for focal therapy *Urology* **72** S12–24

Scherr D S, Eastham J, Ohori M and Scardino P T 2002 Prostate biopsy techniques and indications: when, where, and how? *Semin. Urol. Oncol.* **20** 18–31

Schouten M G, Bomers J G, Yakar D, Huisman H, Rothgang E, Bosboom D, Scheenen T W, Misra S and Futterer J J 2012 Evaluation of a robotic technique for transrectal MRI-guided prostate biopsies *Eur. Radiol.* **22** 476–83

Seifabadi R, Song S E, Krieger A, Cho N B, Tokuda J, Fichtinger G and Iordachita I 2012 Robotic system for MRI-guided prostate biopsy: feasibility of teleoperated needle insertion and ex vivo phantom study *Int. J. Comput. Assist. Radiol. Surg.* **7** 181–90

Song S, Hata N, Iordachita I, Fichtinger G, Tempany C and Tokuda J 2012 A workspace-oriented needle guiding robot for 3T MRI-guided transperineal prostate intervention: evaluation of in-bore workspace and MRI compatibility *Int. J. Med. Robot. Comput. Assist. Surg.* (available online, doi:10.1002/rcs.1430)

Susil R C, Camphausen K, Choyke P, McVeigh E R, Gustafson G S, Ning H, Miller R W, Atalar E, Coleman C N and Menard C 2004 System for prostate brachytherapy and biopsy in a standard 1.5 T MRI scanner *Magn. Reson. Med.* **52** 683–7

Susil R C, Krieger A, Derbyshire J A, Tanacs A, Whitcomb L L, Fichtinger G and Atalar E 2003 System for MR image-guided prostate interventions: canine study *Radiology* **228** 886–94

Susil R C, Menard C, Krieger A, Coleman J A, Camphausen K, Choyke P, Fichtinger G, Whitcomb L L, Coleman C N and Atalar E 2006 Transrectal prostate biopsy and fiducial marker placement in a standard 1.5 T magnetic resonance imaging scanner *J. Urol.* **175** 113–20

Ukimura O, Hirahara N, Fujihara A, Yamada T, Iwata T, Kamoi K, Okihara K, Ito H, Nishimura T and Miki T 2010 Technique for a hybrid system of real-time transrectal ultrasound with preoperative magnetic resonance imaging in the guidance of targeted prostate biopsy *Int. J. Urol.* **17** 890–3

van den Bosch M, Moman M, van Vulpen M, Battermann J, Duiveman E, van Schelven L, de Leeuw H, Lagendijk J and Moerland M 2010 MRI-guided robotic system for transperineal prostate interventions: proof of principle *Phys. Med. Biol.* **55** N133–40

Woodrum D A, Gorny K R, Mynderse L A, Amrami K K, Felmlee J P, Bjarnason H, Garcia-Medina O I, McNichols R J, Atwell T D and Callstrom M R 2010 Feasibility of 3.0 T magnetic resonance imaging-guided laser ablation of a cadaveric prostate *Urology* **75** 1514–6

Yakar D, Schouten M G, Bosboom D G, Barentsz J O, Scheenen T W and Futterer J J 2011 Feasibility of a pneumatically actuated MR-compatible robot for transrectal prostate biopsy guidance *Radiology* **260** 241–7

Zangos S *et al* 2005 MR-guided transgluteal biopsies with an open low-field system in patients with clinically suspected prostate cancer: technique and preliminary results *Eur. Radiol.* **15** 174–82

Zangos S *et al* 2011 MR-compatible assistance system for biopsy in a high-field-strength system: initial results in patients with suspicious prostate lesions *Radiology* **259** 903–10